The role of annealing and synthesis conditions on the optical and morphological characteristics of CuO porous nanofilms

HOSSEIN AKBARI[a*], YASHAR AZIZIAN-KALANDARAGH[b,c*]
[a]*Department of Physics Ardabil Branch, Islamic Azad University, Ardabil, Iran*
[b]*Department of Physics, University of Mohaghegh Ardabili, P.O. Box 179, Ardabil, Iran*
[c]*Department of Engineering Sciences, Sabalan University of Advanced Technologies (SUAT), Namin, Iran*

CuO-PVA nanocomposite films were prepared successfully by sol-gel method with $Cu(CH_3COO)_2.H_2O$ as a precursor and Poly vinyl alcohol(PVA) in aqueous solution. The effect of annealing conditions such as annealing temperature and rate of annealing temperature, immersion cycle, and dip coating speed on the optical, film thickness, and particle size of CuO nanocomposite films has been studied by field emission scanning electron microscopy (FE-SEM), and UV-Visible spectroscopy techniques. According to the FE-SEM results, the sizes of the CuO nanostructures are below 20nm for annealing temperature of about 350 and 500°C. By analyzing the results obtained from the UV-Visible spectrum of the as-prepared CuO nanocomposites a blue shift in band gap energy observed. The blue shift is due to the quantum confined charge carriers in very small nanometer-sized space.

(Received September 6, 2017; accepted April 5, 2018)

Keywords: CuO-PVA Nanocomposite, Sol-Gel Technique, Band Gap, Thin Film

1. Introduction

The semiconductor metal oxide, such as TiO_2, ZnO, Fe_3O_4, Fe_2O_3, Co_3O_4, Bi_2O_3, PbO, CuO and CdO has attracted much attention in the recent year because of their size dependent optical, electronically and structural properties [1-12]. Among all the metal oxide, Copper compound have attracted more attention due to unique potential in optics and optoelectronics [13], electrochemical and catalysts [14], electrochromics [15], solar cells [16-18] and gas sensor applications [19]. There are two well-known copper oxides: Cu_2^+O (Cuprite) and $Cu^{2+}O$ (Tenorite) [20]. CuO is a monoclinic p-type semiconductor with a narrow direct band gap between 1.9-2.1 eV and its considered in terms of transition metal oxides, Where as Cu_2O is a cubic P-type semiconductor with direct band gap around 2-2.6 eV [21,22]. CuO is a promising semiconductor for selective solar absorber since it has a high solar absorber and low thermal emittance in a visible range [23]. A rich variety of technique has been used extensively for the preparation of CuO nanofilms such as: Chemical deposition [24], reactive evaporation [25], sputtering [26,27], spray pyrolysis [28], microwave irradiation [29], and sol-gel [4, 17, 23, 30]. However, among all of techniques, the sol-gel process is particularly attractive because of the following reasons: good homogeneity, ease of composition control, low processing temperature, large area coating, low equipment coat and good optical properties. There are very few reports in the literatures on the synthesis of nanocrystalline copper oxide thin films by sol-gel method. Ozer [31], and Neskovska [32], co-authors to have been prepared Cu_2O thin films with electrochromic exhibit. Electrochromic materials are able to reversibly change their optical properties by an external voltage. Ray has been investigated the optical properties of copper oxide thin films in different annealing temperature and has found Cu_2O phase at 360 °C with a direct band gap of 2.1eV and CuO phase at 400 °C with 1.9 eV [17]. Armelao and co-authors [33], also have been studied on the optical and structural properties of CuO thin films in various temperatures with a different annealing atmosphere. Distinct crystalline phase (Cu_2O and CuO) was observed as a function of annealing conditions (temperature and atmosphere). In this paper, we present a novel route to prepared CuO nanocomposite films through the PVA matrix assistant sol-gel method. Besides, the effect of annealing conditions such as annealing temperature and rate of annealing heating, immersion cycle, and dip coating speed on the optical, film thickness, and particle size of CuO nanocomposite films has been studied by XRD, FESEM, and UV-Vis techniques.

2. Experimental

2.1. Characterization

X-ray diffraction (XRD) patterns were recorded by a Philips-X'PertPro, X-ray diffractometer using Ni-filtered Cu Kα radiation at scan range of $10<2\theta<80$. Field emission scanning electron microscopy, FESEM-HITACHI(S-4160), equipped with an energy-dispersive X-ray spectroscopy (EDX-15kV) was performed to determine the thickness and composition of annealed CuO nanocomposite films. UV-Vis spectroscopy (Varian-Cary100) was used to investigate the optical properties

(Transmit ion and absorption) of the films in the wavelength range of 300-800 nm.

2.2. Synthesis of CuO nanocomposite films

Firstly, 500 mg of Cu $(CH_3COO)_2$. H_2O was dissolved in 50 ml distilled water under stirring at room temperature to be a homogeneous solution. When the color of solution changed to pale blue, an emulsion containing copper nanoparticles have been formed. Then 6 g of poly vinyl alcohol was dissolved in 100 ml distilled water. Solution was left for 24 h at room temperature for ageing the viscosity and then gradually was added to the Cu solution to product CuO nanocrystalline films with well adherent to the substrate. After that, the glass was immersing with 9, 11, and 20 cycle at dip coating speed 10 cm/min in CuO-PVA solution in order to make thin film. The coated nanocomposite films were dried at 100 °C in the air for 10 min after each cycle to be obtained crack free layers. The process above was repeated for more time to obtain required nanocomposite film thickness. The CuO films were annealed at temperatures 350, 500, and 650°C in air for 1 h.

3. Results and discussion

Fig.1. Show the XRD patterns of CuO nanocomposite film at various annealing temperatures. Extremely broaden reflection peaks were observed in Fig. 1, which indicated fine particle nature of the obtained CuO nanocomposite. No other crystalline phases were detected in the calcined product. Two strong peaks located at $2\theta = 35.5^\circ$ and 38.70° are attributed to monoclinic phase of CuO corresponding to $(\bar{1}11)$ and (111) planes, respectively.

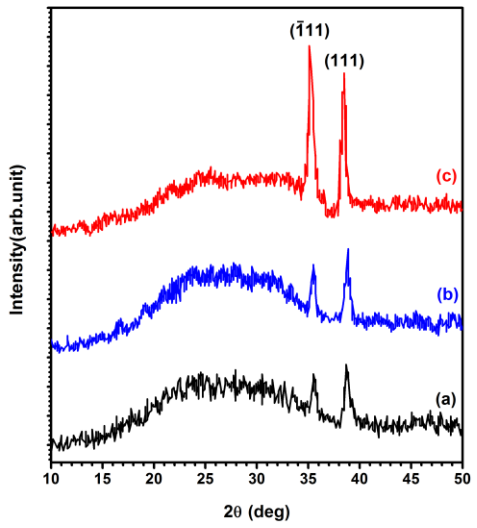

Fig.1. XRD patterns of CuO oxidized thin films annealed (a) 350°C (b) 500°C (c) 650°C.

From XRD data, the crystallite diameter (D_c) of CuO nanocomposite obtained from annealing at 350 and 500 °C was calculated to be 14 and 18 nm, respectively by using the Scherer equation (1).

$$D_c = K\lambda/\beta\cos\theta \quad (1)$$

where β is the breadth of the observed diffraction line at its half intensity maximum (111), K is the so-called shape factor, which usually takes a value of about 0.9, and λ is the wavelength of X-ray source used in XRD. Moreover, increases in the annealing temperature to 650 °C result in increase intensity of the diffraction peaks (Fig. 1c). The FESEM and cross sectional images of CuO nanocomposite films prepare at immersion cycle 9, 11, and 20 and annealing temperature 350 °C and dip coating speed 10 cm/min are shown in the Fig. 2a, 2b, and 2c, respectively. CuO nanocomposite film consists of nanoparticles with particle size about 20–25 nm (Fig. 2a). Increase the immersion cycles from 9 to 11, and then 20 cause agglomeration CuO nanoparticles and increase CuO nanocomposite film porosity due to growing of film thickness. Fig. 2d, 2e, and 2f show the cross-sectional images of CuO nanocomposite at immersion cycle 9, 11, and 20, respectively. It seems film thickness is around 106, 160, and 226 nm for immersion cycle 9, 11, and 20, respectively. Increase in immersion cycle result in increase cross-sectional of CuO nanoparticles films. Fig. 3 shows the optical absorption spectra of CuO nanocomposite films at immersion cycle 9, 11, and 20 with 10 cm min^{-1} dip coating speed. It was observed that all films behave as opaque films between 300-600 nm wavelength range because of absorption values at this wavelength are high and behave as a transparent film higher than 600 nm wavelengths. Increase the immersion cycle leads to increase in the film thickness due to particles growth which causes a shift in the optical absorption edge, consequently, will change the energy band gap of CuO nanocomposite films. The energy band gap values for CuO nanocomposite films versus photon energy ($h\upsilon$) were determined based on the following relations [34]:

$$\alpha h\upsilon = B\,(h\upsilon - E_g)^{m/2} \quad (1)$$

where B is constant, E_g is the band gap, m is another constant which depends on the nature of the transition (m=1 for direct allowed transition) and α is the absorption coefficient which can be determined by [35]:

$$\alpha = \frac{1}{d}\ln\left(\frac{T}{100}\right) \quad (2)$$

where d is the films thickness and T is the transmission data.

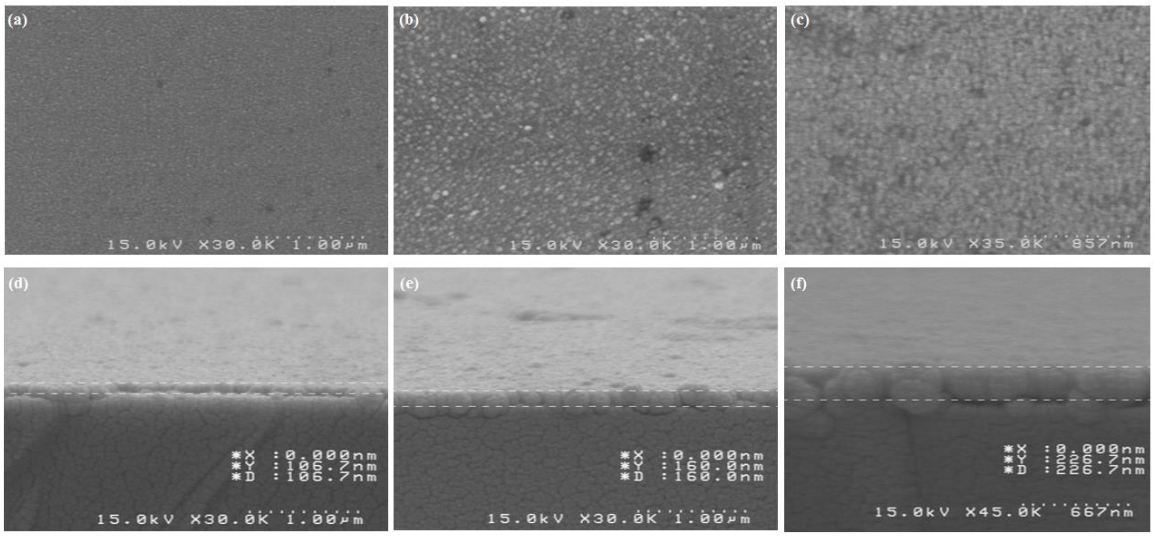

Fig. 2. FESEM and cross sectional images of CuO films with various immersion cycle (a) 9 (b) 11 (c) 20 cycles and respectively their thickness at 350°C (d) 106 nm (e) 160 nm (f) 226 nm.

The energy band gap can be estimated from a plot of $(\alpha h\upsilon)^2$ versus photon energy ($h\upsilon$) when the best straight line can be determined from the slope of the linear part of $(\alpha h\upsilon)^2$ versus $h\upsilon$ axis. The energy band gap of CuO nanocomposite films has a blue shift due to a particles growth (Fig. 3b). The E_g of CuO nanocomposite films are 2.2, 2.13, and 2.03 eV for 9, 11, and 20 cycles, respectively. FESEM images of CuO nanocomposite films at different annealing temperature and heating rate are shown in Fig. 4a, 4b, and 4c. As a result, the Porosity of CuO nanocomposite films strongly changed as a function of annealing temperature and heating rate. It can be seen, surface of CuO nanocomposite annealed at 350°C (HR = 10 °C min^{-1}) is more rough than surface of CuO nanocomposite annealed at 500 °C (HR=2 °C min^{-1}) due to quick vaporization of heavy PVA molecules from the thin films surface in 500 °C than 350 °C. Furthermore, evaporation processes was quiet in low heating rate and particles have enough time to the joint each other to the creation a smooth layer. Fig. 4d, 4e, and 4f show the cross-sectional images of CuO nanocomposite at annealing temperature and heating rate 350°C (HR= 10°C min^{-1}), 500°C (HR= 10°C min^{-1}), and 500 °C (HR=2°C min^{-1}), respectively. According to the cross-sectional images, thickens of CuO nanocomposite at 350°C (HR= 10°C min^{-1}), 500°C (HR= 10°C min^{-1}), and 500°C (HR=2°C min^{-1}) are 353, 380, and 273 nm, respectively. Fig. 5 shows the optical absorption spectra of CuO nanocomposite films at annealing temperatures 350 and 500°C in various heating rate with immersion cycle 20 and dip coating speed 10 cm/ min. According to the Fig. 5 CuO nanocomposites has a blue shift due to particles growth. The E_g of CuO nanocomposite films are 2.2, 1.98, and 1.92 eV for 350°C (HR= 10°C min^{-1}), 500°C (HR= 10°C min^{-1}), and 500°C (HR = 2°C min^{-1}), respectively. Fig.6 a and b show the FESEM images of CuO nanocomposite in annealing temperature 500°C (HR = 10°C min^{-1}) and 500°C (HR = 2°C min^{-1}), respectively. According to the Fig.6 a and b particles size of CuO nanocomposite in annealing temperature 500°C (HR=10°C min^{-1}) is smaller than of particles size of CuO nanocomposite in annealing temperature 500°C (HR=2°C min^{-1}). In heating rate HR=2° C min^{-1} particles have enough time to join to each other and create agglomerate nanoparticles.

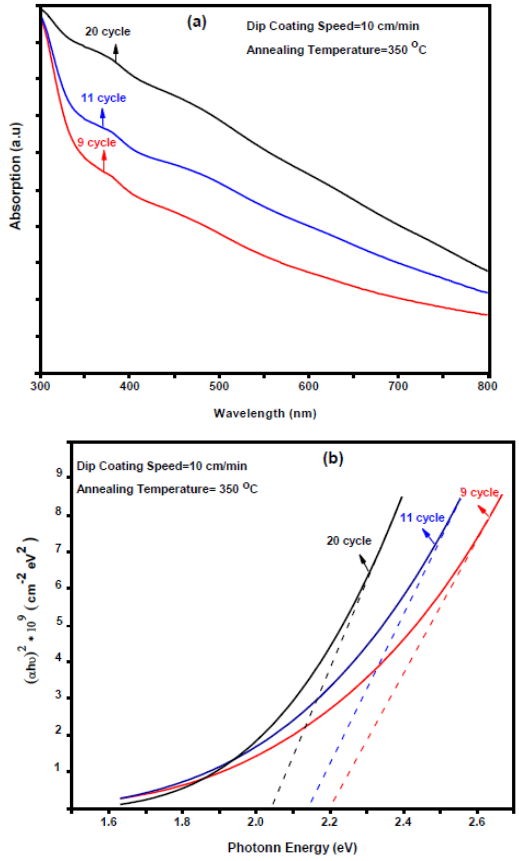

Fig. 3. (a) Absorption spectra and (b) Plot of $(\alpha h\upsilon)^2$ vs photon energy ($h\upsilon$) of CuO thin films at 350°C with various immersion cycle.

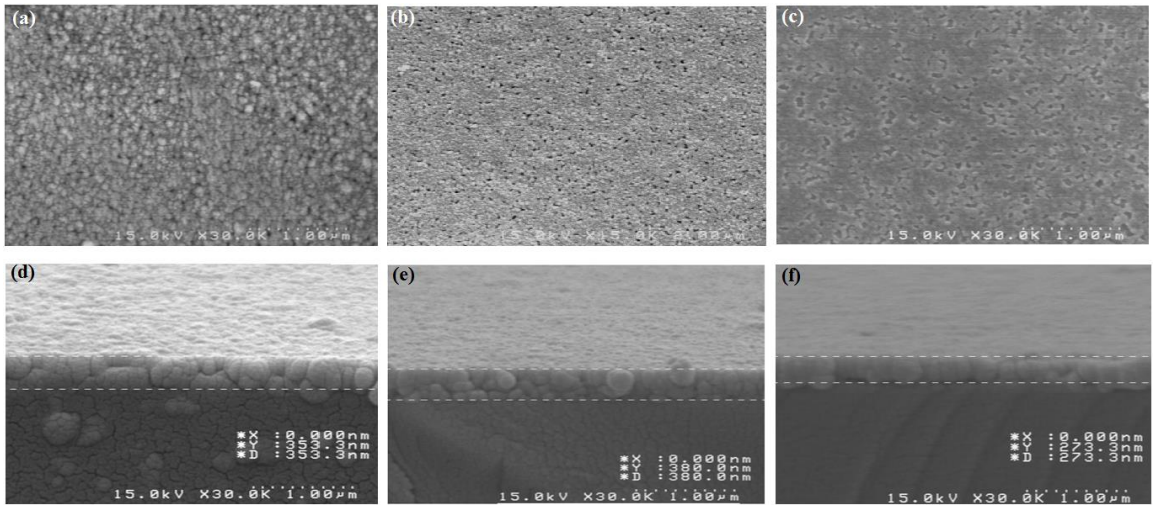

Fig. 4. FE-SEM and cross sectional images of CuO films with various temperature and heating rate (a) 350°C (HR= 10°C min^{-1}) (b) 500°C (HR= 10°C min^{-1}) (c) 500°C (HR=2°C min^{-1}), and respectively their thickness (d) 353 nm (e) 380 nm (f) 273 nm.

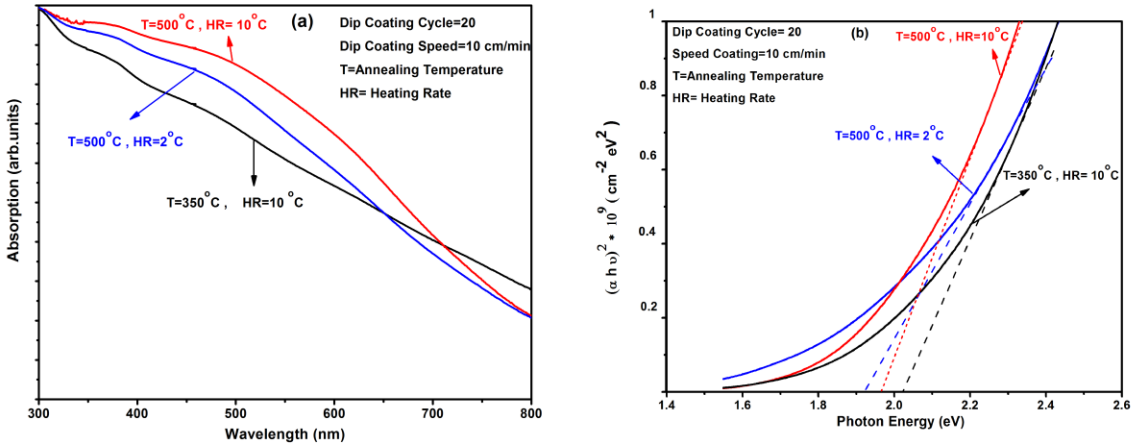

Fig. 5. (a) Absorption spectra and (b) Plot of $(\alpha h\upsilon)^2$ vs photon energy ($h\upsilon$) of CuO thin films at 350 and 500°C in various heating rate with fixed immersion cycle (20 cycles) and dip coating speed (10 cm min^{-1}).

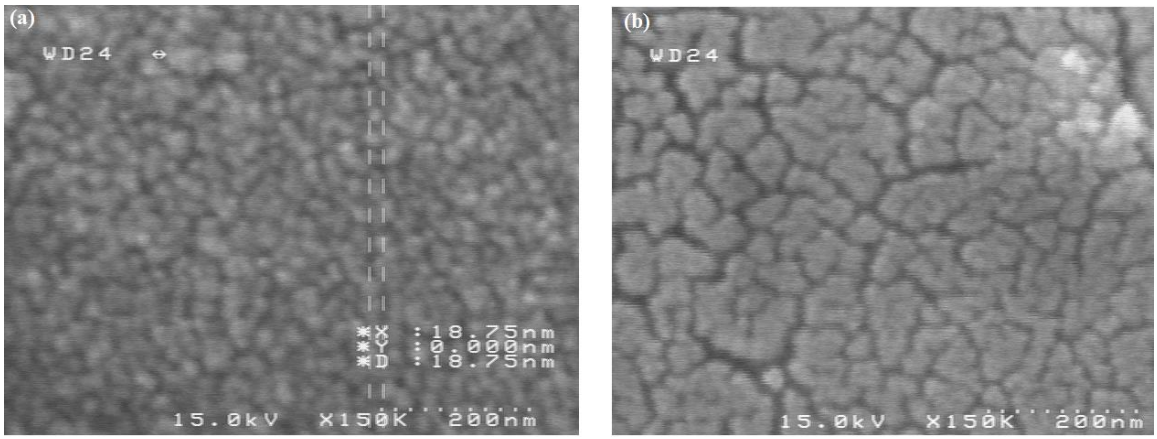

Fig. 6. FESEM image of CuO nanocomposite in annealing temperature (a) 500°C (HR=10 °C min^{-1}) (b) 500°C (HR=2°C min^{-1}).

4. Conclusion

In summary, CuO nanocomposite films were successfully synthesized by PVA matrix assistant sol-gel method. $Cu(CH_3COO)_2.H_2O$ and Poly(Vinyl Alcohol) were used as starting reagents in distilled water. In this paper, we investigated the effect of annealing conditions such as annealing temperature and rate of annealing heating, immersion cycle, and dip coating speed on the optical, film thickness, and particle size of CuO nanocomposite. We found that the energy band gap decrease from 2.2 to 2.03 eV for the films annealed 350°C and same results found with increasing of annealing temperature to 500°C due to an increase of the paticles size. With increasing the immersion cycle and film thickness, a blue shift is observed in the absorption edge and band structure which is due to particles growth and quantum confinement effect. FESEM image show that, increasing in annealing temperature and heating rate cause produced porous CuO nanocomposite film.

References

[1] R. Asahi, T. Morikawa, T. Ohwaki, K. Akoi, Y. Taga, Science **293**, 269 (2001).

[2] M. Shim, P. G. Sionneset, J. AM. Chem. Soc **123**, 11651 (2001).

[3] M. Mahdiani, A. Sobhani, F. Ansari, M. Salavati-Niasari, Journal of Materials Science: Materials in Electronics **28**, 17627 (2017).

[4] R. Shokrani-Havigh, Y. Azizian-Kalandaragh, J. Optoelectron. Adv. M. **19**(3- 4), 283 (2017).

[5] S. Vyas, J. Optoelectron. Adv. M. **19**(11–12), 704 (2017).

[6] M. Dadkhah, F. Ansari, M. Salavati-Niasari, Appl. Phys. A **122,** 700 (2016).

[7] F. Ansari, A. Sobhani, M. Salavati-Niasari, Journal of Colloid and Interface Science **514**(15), 723 (2018).

[8] B. Shaabani, E. Alizadeh-Gheshlaghi, Y. Azizian-Kalandaragh, A. Khodayari, Advanced Powder Technology **25,** 1043 (2014).

[9] K. Ghasemi-Germi, F.Shabani, A. Khodayari, Y. Azizian-Kalandaragh, Synthesis and Reactivity in Inorganic, Metal-Organic, and Nano-Metal Chemistry **44**, 1286 (2014).

[10] N. S. Javan, Y. Azizian-Kalandaragh, A. Khodayari, Optoelectron. Adv. Mat. **7(**9-10), 639 (2013).

[11] J. Hasanzadeh, Y. Azizian-Kalandaragh, A. Khodayari, J. Optoelectron. Adv. M. **14**(5-6), 473 (2012).

[12] C. Sun, X. He, X. Lu, Z. Cao, X. Xie, Optoelectron. Adv. Mat. **11**(11-12), 721 (2017).

[13] M. Caglar, F. Yakuphanoglu, J. Phys. D: Applied.Phys **42**, 045102 (2009).

[14] K. H. Yoon, W. J. Wang, D. H. Kang, Thin Solid Films **372**, 250 (2000).

[15] M. P. Houng, Y. H. Wang, N. F. Wang, W. J. Chang, C. I. Hung, Mater. Chem. Phys **59**, 36 (1999).

[16] S. M. Hosseinpoor-Mashkani, F. Mohandes, M. Salavati-Niasari, K. Venkateswara-Rao, Mater. Res. Bull. **47**, 3148 (2012).

[17] S. M. Hosseinpour-Mashkani, M. Salavati-Niasari, F. Mohandes, K. Venkateswara-Rao, Journal of Materials Science in Semiconductor Processing **16,** 390 (2013).

[18] S. M. Hosseinpour Mashkani, K. Venkateswara Rao, Z. Chamanzadeh, International Conference on Nanoscience Engineering and Technology ICONSET, IEEE, p. 653, 2011.

[19] A. Cruccolini, R. Naducci, R. Palobari, Sensors Actuators B 98, 2004.

[20] A. Richthofer, R. Pomnick, R. Cremer, J. Anal. Chem **358**, 227 (1997).

[21] A. Y. Oral, E. Mensur, M. H. Aslan, E. Basaran, Mater. Chem. Phys **83**, 140 (2004).

[22] J. F. Pierson, A. T. Keck, A. Billard, Applied Surface Science **210**, 359 (2003).

[23] B. Balomurugan, B. R. Mehta, Thin Solid Films **369**, 90 (2000).

[24] T. Maruyama, Solar Energy Mater. Solar Cells **56**, 85 (1998).

[25] F. Lapostolle, A. Billard, J. Vonstebut, Surf. Coat. Technol **135,** 1 (2000).

[26] A. Paretta, M. K. Jayaraj, A. Dinocera, S. Loreti, L. Quercia, A. Agati, Phys. Stat. Sol A **155,** 399 (1996).

[27] S. Ishizuka, T. Maruyama, K. Akimoto, JPN. J. Appl. Phys **39,** L786 (2000).

[28] H. Fan, L. Yang, W. Hua, X. Wu, Z. Wu, S. xie, B. Zou, Nanotechnology **15**, 37 (2004).

[29] H. W. Wang, J. Z. Xu, J. J. Zhu, H. Y. Chen, J. Cryst. Growth **224,** 88 (2002).

[30] R. V. Kumar, R. E. Elgamiel, A. Gedanken, Langmuir **17**, 1406 (2001).

[31] N. Ozer, F. Tepehan, Solar Energy materials and Sollar Cells **30**, 13 (1993).

[32] R. Neskovska, M. Ristova, J. Velevska, M. Ristov, Thin Solid Films **515**, 4717 (2007).

[33] L. Armelao, D. Barrecal and at all, Thin Solid Films **442**, 48 (2003).

[34] N. F. Mott, E. A. Davis, Electronic Process in Non-Crystalline Materials, Clarendon Press, Oxford, 1979.

[35] E. A. Davis, N. F. Mott, Philos, Mag **22**, 903 (1970).

*Corresponding authors: akbari.ph@gmail.com, yashar.a.k@gmail.com